Available online at BCREC Website: http://bcrec.undip.ac.id

Bulletin of Chemical Reaction Engineering & Catalysis, 9 (3), 2014, 156-167

Research Article

One-pot Synthesis of Pt Catalysts Supported on Al-modified TiO_2

Rebecca E. Olsen [1], Calvin H. Bartholomew [2], David B. Enfield [1], Brian F. Woodfield [1]*

[1] *Department of Chemistry and Biochemistry, Brigham Young University, Provo, UT 84602, USA*
[2] *Department of Chemical Engineering, Brigham Young University, Provo, UT 84602, USA*

Received: 20th April 2014; Revised: 14th May 2014; Accepted: 10th June 2014

Abstract

A facile, industrially viable, one-pot synthesis of 0.5-8 wt% Pt supported on 22 mol% Al-modified anatase with high surface area and thermal stability is presented. Four pathways were studied to determine the effects of support properties on catalyst dispersion, and the highest dispersions were observed for high surface area materials containing 5-coordinate anatase. Systematic study of preparation variables shows that low drying temperatures, slow calcination ramp rates, and slow reduction ramp rates further increased Pt dispersion and resulted in a more uniform Pt size distribution. Pt dispersions as high as 54% have been obtained using the one-pot method and 59% for Pt catalysts synthesized by dry impregnation. Statistically designed studies are needed to more completely determine the effects of synthesis variables and to optimize the dispersion and reduction of Pt supported on Al-modified anatase. Results presented in this paper show that this one-pot method and dry impregnation method using our Al-modified anatase support are promising syntheses of highly dispersed Pt supported on stabilized titania. Our results demonstrate that the alumina-stabilized anatase support is superior to other anatase supports for (1) obtaining high Pt dispersions, i.e. more efficiently utilizing this expensive precious metal, and (2) processes in which thermal stability is important due to its constant phase and pore structures at high temperatures.

Keywords: anatase; high surface area; SMSI effect; supported Pt-catalyst; one-pot synthesis

How to Cite: Olsen, R.E., Bartholomew,C.H., Enfield, D.B., Woodfield, B.F. (2014). One-pot Synthesis of Pt Catalysts Supported on Al-modified TiO_2. *Bulletin of Chemical Reaction Engineering & Catalysis*, 9 (3): 156-167. (doi:10.9767/bcrec.9.3.6734.156-167)

Permalink/DOI: http://dx.doi.org/10.9767/bcrec.9.3.6734.156-167

1. Introduction

Noble metals such as Pt supported on anatase TiO_2 are used in a number of oxidation reactions, e.g. oxidation of CO at low temperatures [1], preferential oxidation of CO in H_2/CO mixtures [2], low-temperature, direct synthesis of hydrogen peroxide [3], selective oxidation of primary C–H bonds [4], and oxidation of alcohols to aldehydes [5]. With increasing concerns about atmospheric pollution, there has been significant interest in using catalysts supported on TiO_2 for the complete oxidation of volatile organic compounds to CO_2 and H_2O [6]. A comprehensive review [7] addresses other reactions involving catalysts supported on TiO_2.

In typical syntheses of supported Pt catalysts (i.e. wet and dry impregnation, ion exchange, and strong electrostatic adsorption) an aqueous Pt precursor is prepared and deposited onto a catalyst support, followed by calcination

* Corresponding Author.
E-mail: Brian_Woodfield@byu.edu (B. Woodfield),
Telp: +1 801-422-2093. Fax +1 801-4220153

and then reduction to obtain a Pt metal catalyst [8-11]. Complex synthesis methods may include (1) solution based reductions of Pt precursors [12] and (2) gaseous chemical vapor deposition on supports [13]. These latter complex syntheses may improve catalytic performance; however, they are often time-consuming and expensive processes, which may include multiple steps, low metal loadings per step, and the use of templates which may need to be removed.

Simplified one-pot syntheses of supported Pt catalysts have been previously reported [14-19] in which precursors for the support and Pt catalyst are mixed together. However, many of these one-pot methods encounter difficulties including the formation of large metal crystallites with a broad size distribution and formation of mixed phases between the support and active metal. Therefore, advances in simple, efficient, and industrially viable synthesis methods of supported noble metal catalysts are needed.

The efficiency of Pt use (i.e. Pt dispersion), catalyst activity and selectivity, and catalyst durability are largely dependent on support properties, including crystallite size, surface area, porosity, pore diameter, and stability. For example, increasing the surface area and controlling the porosity and morphology of the support can lead to improved supported catalysts. While previous studies have examined effects of support type (e.g. Al_2O_3, SiO_2, TiO_2), few have examined the effects of altering the properties of a single support, likely due to the availability of commercial supports. The ability to tailor a commercial support to improve its properties is limited.

We previously reported a facile method to synthesize pure and modified anatase TiO_2 with high surface area, thermal stability, and pore volume while controlling pore diameter over a significant range [20]. We report here a one-pot synthesis of supported Pt catalysts, which involves an adaptation to the previous method. This method is referred to as "one-pot" because it involves the addition of the Pt catalyst precursor to the TiO_2 support precursor before calcination. Though similar to sol-gel techniques, this method is solvent deficient. See reference 20 for further discussion. In this study we examine four pathways in a one-pot synthesis method and compare the resulting Pt dispersions with traditional Pt loading methods including dry impregnation (DI) and strong electrostatic adsorption (SEA). Each pathway influences the properties of both the anatase support and the Pt dispersion. Two promising one-pot pathways and the DI method were further examined to determine how the drying temperature, calcination ramp rate, and reduction ramp rate affected the Pt dispersion, crystallite size, and crystallite size distribution. Results presented in this paper show that this simple, fast, industrially viable, one-pot synthesis and the DI method using our Al-modified anatase support are promising syntheses of highly dispersed Pt supported on stabilized titania. Further studies, including statistically designed experiments are needed to (1) more completely determine the effects of synthesis variables, (2) optimize the dispersion and reduction of Pt supported on 22 mol% Al-modified anatase, and (3) determine the activity and selectivity of these catalysts.

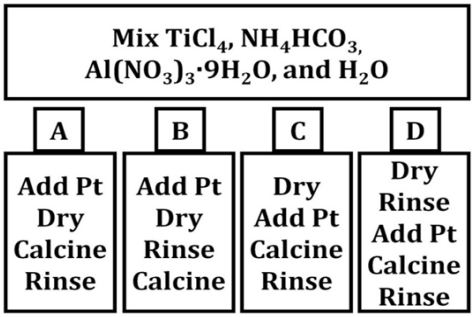

Scheme 1. Synthesis routes of 3 wt% Pt catalysts supported on 22 mol% Al-modified anatase. Pt = $PtCl_4 \cdot xH_2O$.

2. Materials and Methods

2.1. Sample Preparation

0.5-8 wt% Pt catalysts supported on anatase and anatase modified with 22 mol% Al samples were prepared following a general solvent deficient method that can be used to synthesize many metal and mixed metal oxides [20, 21]. A schematic of the synthesis is found in Scheme 1. Approximately 2.86 ml $TiCl_4$, 2.75 g $Al(NO_3)_3 \cdot 9H_2O$, and 10.54 g NH_4HCO_3 (ABC) were mixed together. $PtCl_4 \cdot xH_2O$ was added when specified in the schematic, with the amount of $PtCl_4 \cdot xH_2O$ chosen to obtain the desired Pt loading. 10 ml distilled water was added slowly while stirring to start the reaction and facilitate mixing. The slurry was mixed for five minutes to form a stabilized anatase precursor. The precursor was then dried in air at temperatures of 21 °C or 100 °C for 24+ hours. Samples were rinsed using a vacuum filtration system at room temperature and calcined at 400 °C for three hours in air (ramp rates of 1, 19 °C/min) in the order specified in the synthesis schematic. Samples synthesized via path-

ways A, C, and D were rinsed with 2 L of distilled water while samples synthesized via pathway B were rinsed with 500 ml dilute NH_4OH (1:4 NH_4OH : distilled H_2O) to prevent loss of Pt. Samples were also prepared by dry impregnation (DI) and strong electrostatic adsorption (SEA) [9] for comparison. DI samples were prepared by dissolving $PtCl_4 \cdot XH_2O$ in enough distilled water to fill the pores of the anatase support sample. The Pt mixture was then mixed with the anatase support and dried at room temperature for 24 hours prior to calcination. SEA samples were prepared following the procedure outlined in reference 9. The PZC of the Al-modified anatase was not determined. Instead, the PZC of pure anatase as determined by reference 9 was used. Anatase supports used for the DI and SEA supported catalysts were synthesized following pathway B, without adding Pt. Supports were rinsed with 2 L distilled H_2O before calcination. Details of the support preparation are available elsewhere [20].

2.2. Sample Characterization

X-ray diffraction patterns were collected using a PANalytical X'Pert Pro diffractometer ($Cu\text{-}K_{\alpha 1}$ radiation, λ= 1.540598 Å) at 45 kV and 40 mA over the 2θ range of 10-90 ° at scanning rates of 1.3 °/min. Average crystallite diameters were estimated using the Scherrer equation [22] and confirmed using transmission electron microscopy (TEM). TEM measurements were performed on a Tecnai F20 Analytical STEM operating at 200 keV. The samples were dispersed in ethanol and deposited on copper grids (lacey carbon fiber, 400 mesh copper grids, Ted Pella, Inc.).

The Ti K edge and Pt L_3 edge X-ray absorption spectroscopy spectra (X-ray absorption near edge, XANES, and extended X-ray absorption fine structure, EXAFS) were obtained using the 12-BM-B beamline of the Advanced Photon Source at Argonne National Laboratory. Spectra were collected using a Si(111) crystal monochromator in transmission mode and the spectra were calibrated using Ti or Pt foils as references.

Full-range N_2 sorption isotherms were collected at 77 K using a Micromeritics TriStar 3020 surface analyzer. Samples of 0.25-0.50 g were degassed at 200 °C for 12-24 hours prior to collecting data. Pore volumes were calculated from the adsorption isotherm at a relative pressure of 0.98 and specific surface areas were calculated using the Brunauer-Emmett-Teller (BET) method from a P/P^0 range of 0.05 to 0.2. H2 type pore diameters were calculated using a modified Pierce method [23, 24] with structural corrections for pore area and volume. Pore diameters were calculated from the adsorption branch for H2 type pores, since evaporation of the condensate during desorption is significantly constrained and delayed by the pore necks with "ink-bottle" pore geometry and by the connectivity of the network [25-28]. H3 pore widths were calculated using the newly developed SPG model [29] involving slit geometry for the Kelvin equation, which also incorporates structural corrections for area and volume. For H3 type hysteresis with slit-like pores, the desorption branch is preferred due to delayed condensation observed in the adsorption process [30-33]. For ease of discussion, pore widths and pore diameters will both be referred to as pore diameters.

H_2 chemisorption capacity was measured using a Quantachrome ChemBET TPR/TPD chemisorption Flow Analyzer instrument. Prior to measurements, samples were reduced under H_2 at 250 °C (reduction ramp rates specified in Tables 1-3) for 75 min. Pt reduction temperature was selected based on temperature programmed reductions (TPRs) carried out on a Netzsch STA 409PC instrument. Following reduction, the temperature was reduced to 240 °C under Ar, where samples were held for 30 min to remove loosely bound hydrogen. Samples were cooled in Ar to room temperature. H_2 chemisorption was measured at room temperature. To reverse the suppression of H_2 adsorption by TiO_x species (discussed below), samples were exposed to oxygen at room temperature, following which the oxygen was titrated by H_2. Pt dispersion was calculated using the following stoichiometry:

Reduced and cooled in Ar:

$$H_2 + 2\ Pt \rightleftarrows 2\ Pt{-}H$$

After exposure to oxygen:

$$H_2 \rightleftarrows 2\ H$$

$$PtO + 3\ H \rightleftarrows Pt{-}H + H_2O$$

3. Results and Discussion

3.1. 6.5-8 wt% Pt Samples

Characterizing supported catalysts is a challenge, as complex mixtures or structures often result from the synthesis, which may be further complicated by small crystallite sizes. As seen in Figure 1, Pt peaks are evident in the XRD patterns, with no evidence of an interme-

tallic compound Pt_3Ti. The presence of Pt peaks reveal crystalline Pt particles large enough to be observed by XRD (approx 4-9 nm for pathways B, D, DI, and SEA, approx 28 nm for pathways A and C, determined by the Scherrer formula [22]) in addition to the small and finely dispersed Pt crystallites observed by TEM. The TiO_2 supports for samples synthesized via pathways A and C match anatase TiO_2. The TiO_2 supports for samples synthesized via pathways B, D, DI, and SEA appear nearly amorphous according to XRD. However, TEM analysis reveals crystalline materials of very small (2 nm or smaller) crystallite sizes. No phase associated with the Al modifier is observed in XRD. We conjecture that the Al is present as (a) surface AlO_x species, and/or (b) Al^{3+} incorporated into empty octahedral sites in the anatase lattice. The structure of the modified anatase support will be further examined in an XAS study.

Temperature programmed reductions were conducted to determine the temperature necessary to fully reduce the Pt catalyst. The reduction profile varied between sample pathways, however, to simplify the comparison between sample pathways and synthesis variables, 250° C, the highest temperature needed to fully reduce Pt, was selected. XAS spectroscopy confirmed the complete reduction of Pt to the metallic state. Representative spectra compared with a Pt foil standard are shown in Figure 2.

Following calcination, H_2 chemisorption capacity was measured. Due to the small and finely dispersed nature, Pt crystallites were formed during calcination at 400 °C, probably due to decomposition of Pt oxide, and chemisorbed considerable H_2 (Figure 3). Following reduction at 250 °C, H_2 chemisorption was almost completely suppressed for samples synthesized via pathways B, D, DI, and SEA, and partially suppressed for samples synthesized pathways A and C. However, following subsequent treatment with oxygen, the H_2 chemisorption capacity was restored (Figure 3). The suppression of H_2 uptake after high temperature reduction and the restoration of H_2 chemisorption capacity on Pt and other Group VIII metals after exposure to oxygen have been widely reported in the literature, although the mechanism by which it occurs is not well understood [34-40]. Previous reports postulate that H atoms, which spill over to the support from Pt crystallites, reduce TiO_2 to TiO_x ($x < 2$) species that migrate to the surface and form thin films that block adsorption sites on Pt metal particles [35, 36, 38-40]. Exposure to oxygen reoxidizes the TiO_x thin films to 3-dimensional TiO_2 crystallites, thereby re-exposing most of the Pt. This interaction is referred to as a strong metal-support interaction (SMSI) or more properly, a decoration effect (i.e. decoration of the Pt surface by reduced TiO_x species).

In the present study, the SMSI effect is observed after reducing the samples at 250 °C, though most researchers do not report observing the complete SMSI effect below reduction temperatures of 500 °C [34]. While Paal *et al.* [40] observed complete H_2 chemisorption suppression only after reduction at or above 500 °C, they observed reduced TiO_x species at reduction temperatures as low as 300 °C [40]. Pesty *et al.* [39] however, reported the appearance of partially reduced TiO_x species as well as the initiation of the SMSI effect at temperatures as

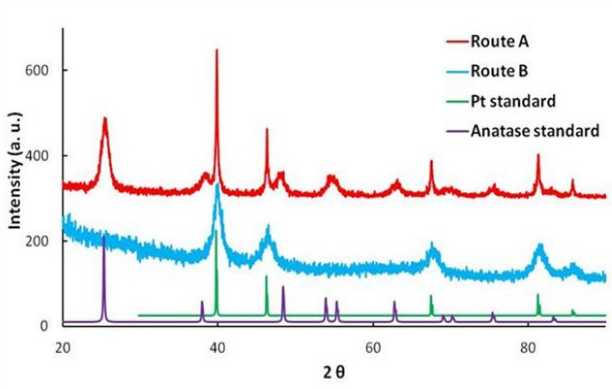

Figure 1. Representative X-ray diffraction patterns of 3 wt% Pt supported on 22 mol% Al synthesized via (a) route B (rinsed prior to calcination) and (b) route A (rinsed after calcination).

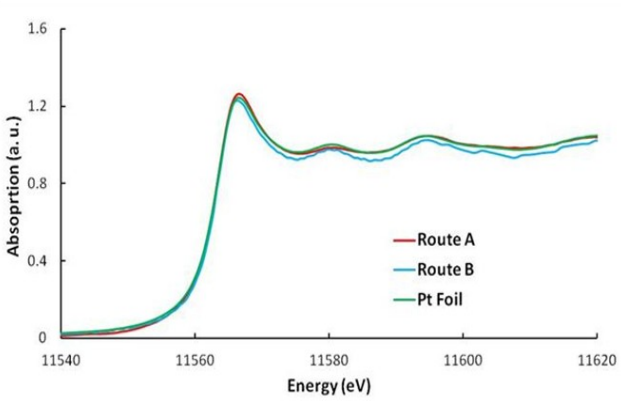

Figure 2. Representative XAS spectra of the Pt L_3 edge of 3 wt% Pt supported on 22 mol% Al-modified anatase synthesized via (a) route B (rinsed prior to calcination), (b) route A (rinsed after calcination) and (c) Pt foil. XAS spectroscopy was used to confirm the reduction of Pt.

low as 177 °C, and the SMSI effect became increasingly apparent as the reduction temperature was increased. We hypothesize that the generally low temperature at which the SMSI effect is observed in the present study could be due to the small crystallite sizes of the anatase support. Additionally, Al modifiers incorporated into the support are likely to induce oxygen defects in order to achieve charge balance. Many researchers have found that oxygen vacancies (or other defects) act as nucleation centers that strongly bind the catalyst, which could therefore lead to interactions between the support and the metal at lower temperatures. Less chemisorption suppression is observed for materials that were not rinsed prior to calcination (pathways A and C). We suspect this is due to the larger anatase and Pt crystallite sizes as well as the different Al-modified anatase crystal structure (discussed below) present in these materials compared with those from the other synthesis pathways (B, D, DI, and SEA). The effects of rinsing on the crystallite structure have been further explored in a companion statistically designed study (manuscript in preparation). However, SMSI states are complex and not fully understood and more studies examining the effects of dopants and the crystallite size of the support on the SMSI effect would be useful. Additionally, the SMSI effect hypotheses in this study are based solely on chemisorption data. Data from additional techniques such as EXAFS and XPS are needed to confirm these hypotheses and will be included in future studies.

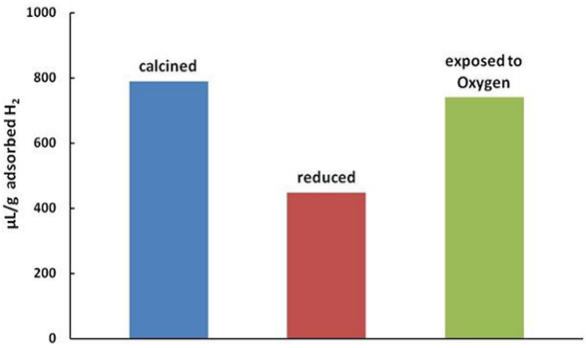

Figure 3. H_2 chemisorption uptakes. Considerable H_2 was adsorbed following calcination. H_2 adsorption was suppressed following reduction due to the SMSI effect. Sample was exposed to oxygen to reverse the SMSI effect and subsequently titrated with H_2. Chemisorption capacity was restored.

The SMSI (or decoration) effect has received attention because the partial coverage of the catalyst by mobile TiO_x species can lead to deactivation of the catalyst for some reactions. Several researchers have presented methods to reverse the SMSI effect through metal catalyst loading techniques and multi-step reduction methods [36, 37]. In the present study, we observed the SMSI effect to be easily reversed by oxygen and therefore these catalysts are of potential use in applications where exposure to oxygen (or water) following reduction is acceptable.

Table 1. Hydrogen uptake by 3 wt% Pt supported on 22 mol% Al-TiO_2 after calcination, reduction, and exposure to O_2.[a]

Synthesis Route	[b]Pt % Dispersion	Surface Area m^2/g	Pore Volume cm^3/g	[c]Pore Diameter nm	Ti Coordination
A	7	136	0.32	8	6
B	15	329	0.26	3.2	5
C	13	163	0.33	8.1	6
D	19	371	0.33	3.2	5
Dry Impregnation (DI)	24	375	0.33	3.2	5
Strong Electrostatic Adsorption (SEA)	18	394	0.35	3.3	5

a Samples were dried at 100 °C, calcined at 400 °C for 3 hours, ramp = 19 °C/min, reduced at 250 °C in H_2 for 75 min, ramp = 2 °C/min, exposed to oxygen, and titrated with H_2 at room temperature.
b. Samples A and B = 8 wt% Pt, all other samples = 6.5 wt% Pt.
c. Pore diameters for materials synthesize via routes A and C were calculated from the desorption branch using the SPG (slit) method, while pore diameters for materials from B, D, DI, and SEA routes were calculated from the adsorption branch using a cylindrical model.

While XRD observations indicate separate metal and support phases present in the reduced catalysts prepared by the one-pot method, hydrogen uptake results in Table 1 reveal, in addition, that (a) Pt metal crystallites are largely accessible to the gas phase and (b) higher Pt dispersions are observed for synthesis pathways B, D, DI, and SEA.

BET data was collected following reduction of the catalyst (Table 1). All materials are Type IV mesoporous materials, and two types of isotherms, H2 and H3, are observed [41]. Representative N_2 sorption isotherms are shown in Figure 4. Pore diameters were calculated using either a cylindrical model [23, 24] or the SPG (slit) model [42] based on the hysteresis of the isotherms as well as mesopore geometry evident in TEM micrographs (Figure 5a). Isotherms of materials synthesized via pathways A and C (not rinsed prior to calcination) are H3 -type, which are associated with slit-like pores (Figure 4); thus pore diameters were calculated from the desorption branch using the SPG model [29-33, 42]. Isotherms for materials synthesized via pathways B, D, DI, and SEA (anatase supports were rinsed prior to calcination) are mainly H2-type, associated with networked, ink-bottle pores; accordingly, these pore diameters were calculated from the adsorption branch using a cylindrical model to avoid problems associated with percolation encountered in the desorption branch [25-28]. It should be noted that while the H3-type materials fit the model quite well, the H2-type materials did not. We suspect the H2-type pores are irregularly shaped with a distribution of pore widths and a range of pores either open to the surface and/or networked (branched).

As seen in Table 1, synthesis pathways B, D, DI, and SEA, (anatase supports rinsed prior to calcination, H2-type pores), lead to higher levels of Pt dispersion than synthesis pathways A and C (anatase supports not rinsed prior to calcination, H3-type pores), likely due to the higher surface areas and smaller pore diameters observed for B, D, DI, and SEA materials (Scheme 1). Further structural analysis using XANES spectroscopy reveals that pathways leading to high Pt dispersions and high surface areas (B, D, DI, and SEA) contain primarily 5-coordinate Ti, while the Ti environment in pathways leading to lower Pt dispersions and lower surface areas (A and C) matched a standard anatase environment, with a Ti-coordination of 6 (see Figure 6). Therefore, we conclude that rinsing affects the pore structure, surface morphology, and crystal structure of anatase supports. A 5-coordinate semi-amorphous precursor to anatase has been reported in the literature [43-47]. We hypothesize that during the rinsing process, some Al migrates from the surface of TiO_2 into empty octahedral sites to stabilize and maintain this 5-coordinate precursor structure during and after calcination. In precursors that are not rinsed before calcination aluminum ions could remain bound to the surface and therefore cannot inhibit grain growth and structural rearrangement to the 6-coordinate structure of anatase during calcination. Although the 5-coordinate materials presented in this study appear largely amorphous to XRD (i.e., observed as broad, low intensity peaks), TEM micrographs reveal that these materials are not truly amorphous, but instead contain small crystallites of approximately 2 nm or less (Figure 5b). Moreover, from the XRD patterns, these 5-coordinate materials appear to be anatase-like.

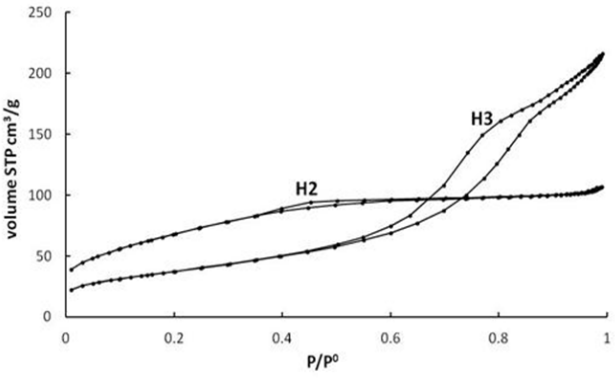

Figure 4. N_2 sorption isotherm examples. H3 type (slit-like pores) is representative of materials synthesized via routes A and C. H2 type (networked pores) are representative of materials synthesized via routes B, D, DI, and SEA. The types of pore structures demonstrates the effect of rinsing on the pore structure.

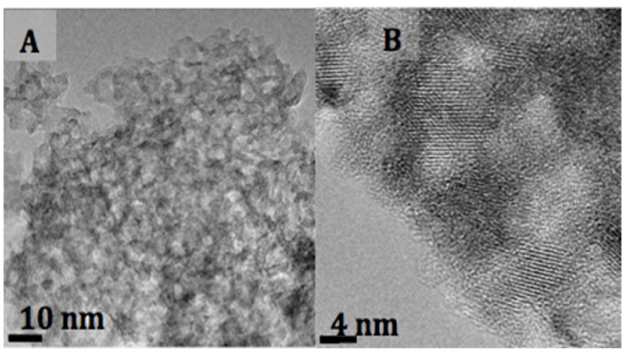

Figure 5. TEM micrographs of 22 mol% Al-modified anatase calcined at 400 °C highlighting A) Mesoporous geometry and B) 2 nm crystallites.

We conclude that 5-coordinate Ti is inherent to small crystallites with limited 3D connectivity and which therefore contain a large percentage of surface Ti atoms. Lattice changes induced by the Al modifier, including strain and oxygen deficiency to achieve charge balance, could also affect the Ti-coordination. In a companion study we will further analyze the structure of the modified anatase using X-ray absorption spectroscopy.

Though initial Pt dispersions obtained using our method were promisingly high for such high Pt wt% loadings, large Pt crystallites are also observed by TEM among small and finely dispersed Pt crystallites (Figure 7). Thus, Pt was not fully utilized. Therefore, three synthesis pathways, B, D, and DI, were further studied to determine if variations in drying temperature, calcination ramp rate, and reduction ramp rate affect Pt crystallite size and dispersion. Results in Table 2 show that low drying temperatures (slow drying rates) and slow calcination ramp rates lead to smaller Pt crystallites and higher Pt dispersions compared with high drying temperatures and fast calcination ramp rates. We hypothesize that at slower drying rates smaller Pt nuclei are formed, while at slower calcination ramp rates the water partial pressure is lower enabling formation of smaller crystallites and decreased cluster and crystal-

Table 2. Effects of drying temperature, calcination ramp rate, and reduction ramp rate on Pt dispersion of a 6.5-8 wt% Pt catalyst supported on 22 mol% Al-TiO_2 after calcination, reduction, and exposure to O_2.[a]

Synthesis Route [a]	Drying Temp °C	Calcination Ramp Rate °C/min	Reduction Ramp Rate °C/min	Pt % Dispersion [b]
B	21	1	1	25
	100	19	2	15
DI	21	1	1	30
	100	19	1	20
	100	19	2	24
D	100	19	1	19
	100	19	2	19

a. Samples were dried at 25 °C or 100 °C, calcined at 400 °C for 3 hours, ramp = 1 or 19 °C/min, reduced at 250 °C in H_2 for 75 min, ramp = 1 or 2 °C/min, exposed to oxygen, and titrated with H_2 at room temperature.
b. Sample B = 8 wt% Pt, Samples DI and D = 6.5 wt% Pt

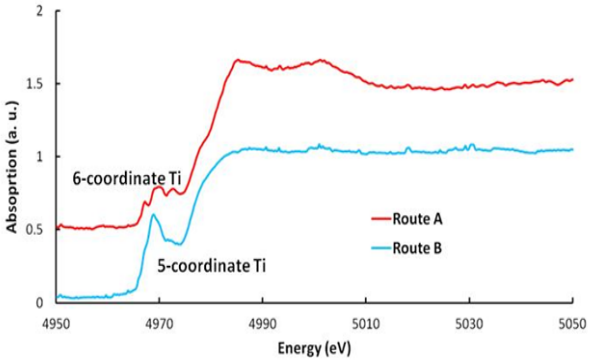

Figure 6. Representative XANES spectra of the Ti K-edge 3 wt% Pt supported on 22 mol% Al-modified anatase synthesized via (a) route B (rinsed prior to calcination), (b) route A (rinsed after calcination). XANES spectra reveal 5-coordinate Ti for samples rinsed prior to calcination and 6-coordinate Ti for samples only rinsed after calcination.

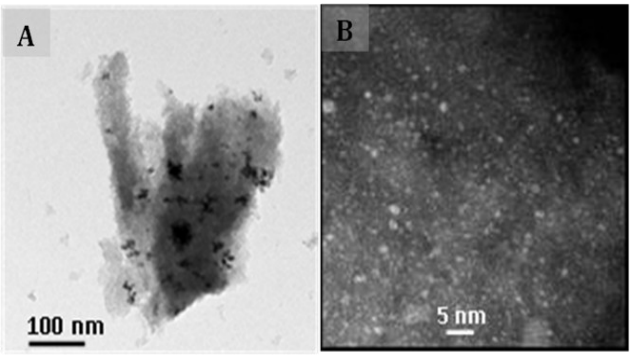

Figure 7. TEM micrographs of 6.5 wt% Pt supported on 22 mol% Al-modified anatase synthesized with drying temperature = 100°C, calcination ramp rate = 19°C/min, and reduction ramp rate = 2°C/min. A) Large Pt crystallites among B) finely dispersed Pt are evident.

lite migration rates. The effects of reduction rates are inconclusive from these limited experiments. In the case of the DI pathway, increasing the reduction ramp rate increases Pt dispersion, while in pathway D, the reduction ramp rate did not affect Pt dispersion. More studies are needed to determine the effect of reduction ramp rate, although a wealth of previous literature indicates that slow reduction rates are associated with higher dispersion [48]. While the highest dispersions obtained were achieved using a low drying temperature, a slow calcination ramp rate, and a slow reduction ramp rate, combinations of fast reduction ramp rates with low drying temperatures and slow calcination ramp rates, which have not yet been examined, may facilitate higher Pt dispersion, although this is unlikely.

TEM micrographs confirm the changes in Pt dispersion with synthesis variations. Figure 8 compares 3 wt.% Pt supported on 22 mol% Al-modified anatase prepared via pathway B with 1) a drying temperature of 21 °C, a calcination ramp rate of 1 °C/min, and a reduction ramp rate of 1 °C/min, and 2) a drying temperature of 100 °C, a calcination ramp rate of 19 °C/min, and a reduction ramp rate of 2 °C/min. Both preparations led to areas of small (approx 2 nm or less), highly dispersed Pt crystallites (Figures 1a and 2a) and some larger Pt crystallites (Figures 1b and 2b). However, conditions used for sample 2 led to a less uniform Pt size distribution, with more prevalent large Pt crystallites of larger diameters (compared with large Pt crystallites in sample 1), and, while the majority of micrographs for sample 1 contained areas of finely dispersed Pt observed in micrographs 1a and 1c, sample 2 has areas with little to no small (2 nm or less) Pt particles and only medium (approx 5 nm) Pt particles present (Figures 2c).

3.2. 0.5 wt% Pt Samples

Based on results from the 6.5-8 wt.% Pt samples, 0.5 wt.% Pt catalysts supported on TiO_2 synthesized via pathways, B, D, and DI, using a drying temperature of 21 °C, a calcination ramp rate of 1 °C/min, and a reduction ramp rate of 1 °C/min were examined. Results in Table 3 reveal that this method results in high Pt disper-

Table 4. Pt dispersion comparison table.

	Sample	Wt.% Pt	Pt % Dispersion	Source
1	$Pt/Na/TiO_2$	0.5	94[c]	[10]
2	$Pt/Li/TiO_2$	0.5	89[c]	[10]
3	Pt/TiO_2	0.6	68.5[d1]	[49]
4	Pt, TiO_2, Al22, DI	0.5	59[d1]	*
5	[a]Pt, TiO_2, Al22, Route B	0.5	54[d1]	*
6	TiO_2	1-3	51-54[c]	[12]
7	Pt/TiO_2	1	52[c]	[50]
8	$Pt\text{-}Re/TiO_2$	0.8	51.9[c]	[51]
9	$Pt/K/TiO_2\text{-}Al_2O_3$	1	51[d]	[52]
10	[b]Pt, TiO_2, Al22, Route B	0.5	45[d1]	*
11	Pt/TiO_2	1	39.1[d1]	[49]
12	$Rh/Pt/MgO/TiO_2$	1	36[e]	[53]
13	Pt-Ba/Al-Ti	2.3	18[b1]	[11]

a. Dispersion calculated prior to O_2 exposure
b. Dispersion calculated following O_2 exposure
c. c CO chemisorption, stoichiometry used was not reported
d. H_2 chemisorption, stoichiometry used was not reported
e. d1. H_2 chemisorption, stoichiometry = 1 Pt : 1 H
f. method of determining Pt dispersion unknown.
*This paper

Table 3. Pt dispersion of a 0.5 wt.% Pt catalyst supported on 22 mol% $Al\text{-}TiO_2$ after calcination, reduction, and exposure to O_2.[a]

[a]Synthesis Route	Drying Temp °C	Calcination Ramp Rate °C/min	Reduction Ramp Rate °C/min	Pt % Dispersion
DI	21	1	1	59
B	21	1	1	[b]45
D	21	1	1	30

a. Samples were dried at 25 °C, calcined at 400 °C for 3 hours, ramp = 1 °C/min, reduced at 250 °C in H_2 for 75 min, ramp = 1 °C/min, exposed to oxygen, and titrated with H_2 at room temperature.
b. Prior to oxygen exposure Pt dispersion = 54%

sions for samples prepared via dry impregnation, demonstrating the excellent properties of the Al-modified TiO_2 support. While pathway D resulted in only moderate Pt dispersions, pathway B resulted in high Pt dispersions. The decoration effect (SMSI) was not as strongly observed for pathway B 0.5 wt.% Pt samples as in prior 6.5-8 wt.% Pt samples. In the case of pathway B (0.5 wt.% Pt samples), Pt dispersions prior to O_2 exposure were significantly higher than after O_2 exposure. Further experimentation is needed to understand this phenomenon.

Table 4 compares Pt dispersions of 0.5 wt.% Pt materials presented in this paper with dispersions of Pt supported on TiO_2 reported with documented methods in the recent literature. Samples (1) and (2) in Table 4 have unusually high Pt dispersions, however these samples contain K and Na making it difficult to compare the products. Additionally, these materials were obtained through a multi-step process which could present difficulties in an industrial setting. Pt dispersions obtained using DI and the one-pot pathway B are higher than the majority of other dispersions reported for similar Pt wt.% loadings. The one pot method shows initial promise, though it must be further optimized to control and increase Pt dispersion and decrease Pt crystallite/cluster size. For example, it is expected that variables such as reaction pH, mixing time, and drying time could affect Pt dispersion.

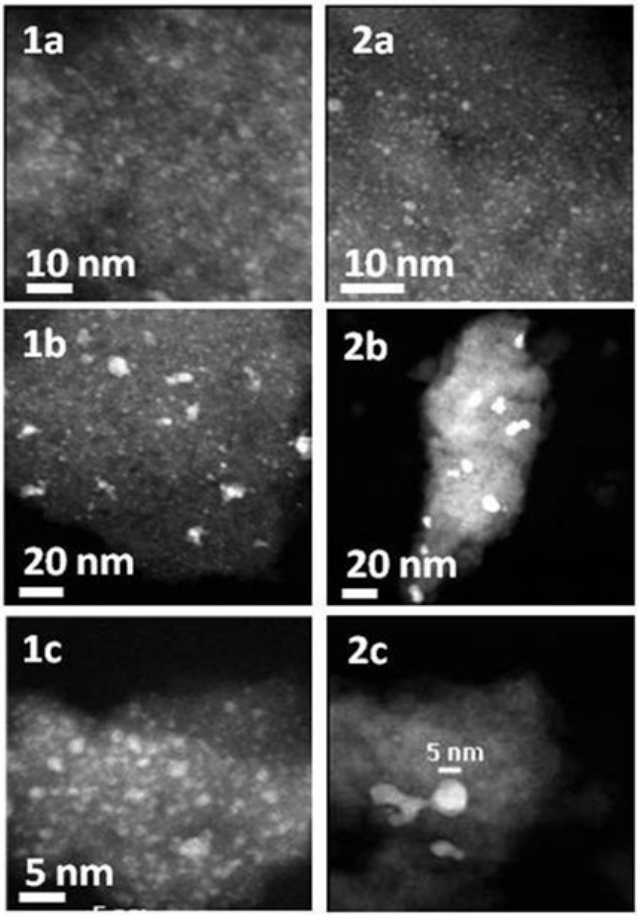

Figure 8. TEM images of 3 wt.% Pt supported on 22 mol% Al-modified anatase synthesized via route B. 1) drying temperature = 25 °C, calcination ramp rate = 1 °C/min, and reduction ramp rate = 1 °C/min. 2) drying temperature = 100 °C, calcination ramp rate = 19 °C/min, and reduction ramp rate = 2 °C/min.

3.3. Method Overview

Results presented in this paper show that the simple, convenient one-pot method and the DI method using our Al-modified anatase support are promising for syntheses of highly dispersed 0.5-8 wt.% Pt supported on stabilized titania. Our results demonstrate that the stabilized anatase support is superior to other anatase supports for 1) obtaining high Pt dispersions, i.e. more efficiently utilizing this expensive precious metal and 2) processes in which thermal stability is important due to its constant phase and pore structures at high temperatures. Initial SEA results (Table 1) indicate promise for this method, and further study of this synthesis pathway is planned. Our systematic study of preparation variables shows that drying temperature, calcination ramp rate, and reduction ramp rate clearly affect the size and dispersion of Pt crystallites on the anatase support (see Table 2). It is expected that other synthesis variables (e.g. pH during impregnation) can affect Pt dispersion, activity, and selectivity. Statistically designed studies are needed to more completely determine the effects of synthesis variables and to optimize the dispersion and reduction of Pt supported on 22 mol% Al-modified anatase. Further work will also include catalytic activity and selectivity tests.

4. Conclusions

We have presented a simple, fast, industrially viable, one-pot synthesis that can be used to prepare 0.5-8 wt.% Pt supported on Al-modified anatase with high surface area and thermal stability. Dispersions for 0.5 wt.% Pt catalysts as high as 54% for a one-pot preparation and 59% for DI on the stabilized anatase support have been obtained which are higher than most previously reported in literature for Pt of comparable loadings.

The SMSI (or decoration) effect, causing blocking of H_2 adsorption sites during H_2 chemisorption, is observed at an unusually low temperature (250 ^oC) for most samples. The low temperature onset may be due to the small crystallite sizes of the anatase support, as well as defects induced by the Al-modifier which could lead to support-metal interactions at lower temperatures. The SMSI effect was easily reversed by oxygen and therefore these catalysts are of potential use in applications where exposure to oxygen (or water) following reduction is acceptable.

Our work shows that support structure due to its preparation by different pathways and a number of synthesis variables affects Pt dispersion. The highest dispersions were observed for samples containing 5 coordinate anatase supports of high surface area, synthesized using a low drying temperature, a slow calcination ramp rate, and a slow reduction ramp rate. Statistically designed studies are needed to more completely understand the effects of drying temperature, calcination ramp rate, reduction ramp rate, and other variables, as well as to optimize the dispersion of Pt onto anatase supports

5. Acknowledgments

Funding for this work was provided by the U.S. Department of Energy grant DE-FG02-05ER15666 and the National Science Foundation grant CHE-0959862. We would like to thank Dr Jeff Farrer and the BYU microscopy laboratory for their assistance with TEM imaging. The XAS work at the Advanced Photon Source at Argonne National Laboratory was supported by the U.S. Department of Energy, Office of Basic Energy Sciences, at the 12-BM beamline (GUP27669).

References

[1] Haruta, M., Tsubota, S., Kobayashi, T., Kageyama, H., Genet, M. J., Delmon, B. (1993). Low-Temperature Oxidation of Carbon Monoxide Over Gold Supported on Titanium Dioxide, Î±-Ferric Oxide, and Cobalt Tetraoxide. *J. Catal.,* 144 (1): 175-192.

[2] Imai, H., Date, M., Tsubota, S. (2008). Preferential Oxidation of CO in H_2-Rich Gas at Low Temperatures over Au Nanoparticles Supported on Metal Oxides. *Catal. Lett.,* 124 (1-2): 68-73.

[3] Edwards, J. K., Carley, A. F., Herzing, A. A., Kiely, C. J., Hutchings, G. J. (2008). Direct Synthesis of Hydrogen Peroxide from H_2 and O_2 Using Supported Au-Pd Catalysts. *Faraday Discuss.,* 138 (Nanoalloys): 225-239.

[4] Kesavan, L., Tiruvalam, R., Ab, R. M. H., bin, S. M. I., Enache, D. I., Jenkins, R. L., Dimitratos, N., Lopez-Sanchez, J. A., Taylor, S. H., Knight, D. W., Kiely, C. J., Hutchings, G. J. (2011). Solvent-Free Oxidation of Primary Carbon-Hydrogen Bonds in Toluene Using Au-Pd Alloy Nanoparticles. *Science (Washington, DC, U. S.),* 331 (6014), 195-199.

[5] Enache, D. I., Edwards, J. K., Landon, P., Solsona-Espriu, B., Carley, A. F., Herzing, A. A., Watanabe, M., Kiely, C. J., Knight, D. W., Hutchings, G. J. (2006). Solvent-Free Oxidation of Primary Alcohols to Aldehydes Using Au-Pd/TiO_2 Catalysts. *Science (Washington, DC, U. S.),* 311 (5759), 362-365.

[6] Tahir, S. F., Koh, C. A. (1996). Catalytic Oxidation for Air Pollution Control. *Environ. Sci. Pollut. Res. Int.,* 3 (1): 20-23.

[7] Carp, O., Huisman, C. L., Reller, A. (2004). Photoinduced Reactivity of Titanium Dioxide. *Prog. Solid State Chem.,* 32 (1-2): 33-177.

[8] Wegener, S. L., Marks, T. J., Stair, P. C. (2011). Design Strategies for the Molecular Level Synthesis of Supported Catalysts. *Acc. Chem. Res.,* 45 (2); 206-214.

[9] Regalbuto, J., Editor, *Catalyst Preparation: Science and Engineering.*, (2007). CRC Press LLC: p 474.

[10] Panagiotopoulou, P., Kondarides, D. I. (2009). Effects of Alkali Promotion of TiO_2 on the Chemisorptive Properties and Water-Gas Shift Activity of Supported Noble Metal Catalysts. *J. Catal.,* 267 (1): 57-66.

[11] Pieta, I. S., Epling, W. S., Garcia-Dieguez, M., Luo, J. Y., Larrubia, M. A., Herrera, M. C., Alemany, L. J. (2011). Nanofibrous Pt-Ba Lean NOx Trap Catalyst with Improved Sulfur Resistance and Thermal Durability. *Catal. Today,* 175 (1): 55-64.

[12] Kimura, K., Einaga, H., Teraoka, Y. (2011). Preparation of Highly Dispersed Platinum Catalysts on Various Oxides by Using Polymer-Protected Nanoparticles. *Catal. Today,* 164 (1): 88-91.

[13] Banis, M. N., Sun, S., Meng, X., Zhang, Y., Wang, Z., Li, R., Cai, M., Sham, T.-K., Sun, X. (2013). $TiSi_2O_x$ Coated N-Doped Carbon Nanotubes as Pt Catalyst Support for the Oxygen Reduction Reaction in PEMFCs. *J. Phys. Chem. C,* 117 (30): 15457-15467.

[14] Rebrov, E. V., Berenguer-Murcia, A., Johnson, B. F. G., Schouten, J. C. (2008). Gold Supported on Mesoporous Titania Thin Films for Application in Microstructured Reactors in Low-Temperature Water-Gas Shift Reaction. *Catal. Today,* 138 (3-4): 210-215.

[15] Muraza, O., Rebrov, E. V., Berenguer-Murcia,

A., de, C. M. H. J. M., Schouten, J. C. (2009). Selectivity Control in Hydrogenation Reactions by Nanoconfinement of Polymetallic Nanoparticles in Mesoporous Thin Films. *Appl. Catal., A,* 368 (1-2): 87-96.

[16] Cao, Y., Zhai, W., Zhang, X., Li, S., Feng, L., Wei, Y. (2012). Mesoporous SiO_2-Supported Pt Nanoparticles for Catalytic Application. *ISRN Nanomater.*, 745397, 8 pp.

[17] Yacou, C., Ayral, A., Giroir-Fendler, A., Baylet, A., Julbe, A. (2010). Catalytic Membrane Materials With a Hierarchical Porosity and Their Performance in Total Oxidation of Propene. *Catal. Today,* 156 (3-4): 216-222.

[18] Liu, S.-H., Chiang, C.-C., Wu, M.-T., Liu, S.-B. (2010). Electrochemical Activity and Durability of Platinum Nanoparticles Supported on Ordered Mesoporous Carbons for Oxygen Reduction Reaction. *Int. J. Hydrogen Energy,* 35 (15): 8149-8154.

[19] Teoh, W. Y., Maedler, L., Beydoun, D., Pratsinis, S. E., Amal, R. (2005). Direct (One-Step) Synthesis of TiO_2 and Pt/TiO_2 Nanoparticles for Photocatalytic Mineralization of Sucrose. *Chem. Eng. Sci.,* 60 (21): 5852-5861.

[20] Olsen, R. E., Bartholomew, C. H., Huang, B., Simmons, C., Woodfield, B. F. (2014). Synthesis and characterization of pure and stabilized mesoporous anatase titanias. *Microporous Mesoporous Mater.,* 184: 7-14.

[21] Woodfield, B. F., Liu, S., Boerio-Goates, J., Liu, Q. (2007). Preparation of Uniform Nanoparticles of Ultra-High Purity Metal Oxides, Mixed Metal Oxides, Metals, and Metal Slloys. WO2007098111A2.

[22] Patterson, A. L. (1939). The Scherrer Formula for X-Ray Particle-Size Determination. *Phys. Rev.,* 56: 978-82.

[23] Pierce, C. (1953). Computation of Pore Sizes From Physical Adsorption Data. *J. Phys. Chem.,* 57: 149-152.

[24] Orr, C., Jr., Dallavalle, J. M. (1959). *Fine Particle Measurement-Size, Surface, and Pore Volume*. Macmillan Co.: p 353 pp.

[25] Liu, H., Zhang, L., Seaton, N. A. (1993). Sorption Hysteresis as a Probe of Pore Structure. *Langmuir,* 9 (10): 2576-2582.

[26] Rojas, F., Kornhauser, I., Felipe, C., Esparza, J. M., Cordero, S., Dominguez, A., Riccardo, J. L. (2002). Capillary Condensation in Heterogeneous Mesoporous Networks Consisting of Variable Connectivity and Pore-Size Correlation. *Phys. Chem. Chem. Phys.,* 4 (11): 2346-2355.

[27] Niemark, A. V. (1991). Percolation Theory of Capillary Hysteresis Phenomena and Its Application for Characterization of Porous Solids. *Stud. Surf. Sci. Catal.,* 62 (Charact. Porous Solids 2): 67-74.

[28] Parlar, M., Yortsos, Y. C. (1988). Percolation Theory of Vapor Adsorption-Desorption Processes in Porous Materials. *J. Colloid Interface Sci.,* 124 (1): 162-176.

[29] Huang, B., Bartholomew, C., H., Woodfield, B. F. (2013). Facile Synthesis of Mesoporous Alumina With Tunable Pore Size: Effects of Alcohols in Precursor Formation and Calcination. *Microporous Mesoporous Mater.,* 177: 37-46.

[30] Ball, P. C., Evans, R. (1989). Temperature Dependence of Gas Adsorption on a Mesoporous Solid: Capillary Criticality and Hysteresis. *Langmuir,* 5 (3): 714-723.

[31] Neimark, A. V., Ravikovitch, P. I. (2001). Capillary Condensation in MMS and Pore Structure Characterization. *Microporous Mesoporous Mater.,* 44-45: 697-707.

[32] Neimark, A. V., Ravikovitch, P. I., Vishnyakov, A. (2000). Adsorption Hysteresis in Nanopores. *Phys. Rev. E: Stat. Phys., Plasmas, Fluids, Relat. Interdiscip. Top.,* 62 (2-A): R1493-R1496.

[33] Monson, P. A. (2008). Contact Angles, Pore Condensation, and Hysteresis: Insights from a Simple Molecular Model. *Langmuir,* 24 (21): 12295-12302.

[34] Tauster, S. J., Fung, S. C., Garten, R. L. (1979). Strong Metal-Support Interactions. Group 8 Noble Metals Supported on Titanium Dioxide. *J. Am. Chem. Soc.,* 100 (1): 170-175.

[35] Stevenson, S. A., Dumesic, J. A., Baker, R. T. K., Ruckenstein, E., Editors. (1987). *Metal-Support Interactions in Catalysis, Sintering, and Redispersion*. Van Nostrand Reinhold Co.: p 315 pp.

[36] Baker, R. T. K., Kim, K. S., Emerson, A. B., Dumesic, J. A. (1986). A Study of the Platinum-Titanium Oxide System for the Hydrogenation of Graphite: Ramifications of Strong Metal-Support Interactions. *J. Phys. Chem.,* 90 (5): 860-866.

[37] Bonanni, S., Ait-Mansour, K., Brune, H., Harbich, W. (2011). Overcoming the Strong Metal-Support Interaction State: CO Oxidation on TiO_2(110)-Supported Pt Nanoclusters. *ACS Catal.,* 1 (4): 385-389.

[38] de la Pena O'Shea, V. A., Consuelo, A. G. M., Platero, P. A. E., Campos-Martin, J. M., Fierro, J. L. G. (2011). Direct Evidence of the SMSI Decoration Effect: the Case of Co/TiO_2 Catalyst. *Chem. Commun. (Cambridge, U. K.),* 47 (25): 7131-7133.

[39] Pesty, F., Steinrueck, H.-P., Madey, T. E. (1995). Thermal Stability of Pt Films on TiO_2(110): Evidence for Encapsulation. *Surf. Sci.,* 339 (1/2): 83-95.

[40] Paal, Z., Menon, P. G., Editors. (1988). *Hydrogen Effects in Catalysis. Fundamentals and Practical Applications.* In: *Chem. Ind. (Dekker), 1988, 31*. Marcel Dekker, Inc.: p 753 pp.

[41] Sing, K. S. W., Everett, D. H., Haul, R. A. W., Moscou, L., Pierotti, R. A., Rouquerol, J., Siemieniewska, T. (1985). Reporting Physisorption Data for Gas/Solid Systems with Special Reference to the Determination of Surface Area and Porosity (Recommendations 1984). *Pure Appl. Chem.,* 57 (4): 603-619.

[42] Huang, B. B., C., Woodfield, B.F. (2014). Improved Calculations of Pore Size Distribution for Relatively Large, Irregular Slit-Shaped Mesopore Structure. *Microporous Mesoporous Mater.,* 184: 112-121.

[43] Chen, L. X., Rajh, T., Wang, Z., Thurnauer, M. C. (1997). XAFS Studies of Surface Structures of TiO_2 Nanoparticles and Photocatalytic Reduction of Metal Ions. *J. Phys. Chem. B,* 101 (50): 10688-10697.

[44] Chen, L. X., Rajh, T., Jager, W., Nedeljkovic, J., Thurnauer, M. C. (1999). X-Ray Absorption Reveals Surface Structure of Titanium Dioxide Nanoparticles. *J. Synchrotron Radiat.,* 6 (3): 445-447.

[45] Luca, V., Djajanti, S., Howe, R. F. (1998). Structural and Electronic Properties of Sol-Gel Titanium Oxides Studied by X-ray Absorption Spectroscopy. *J. Phys. Chem. B,* 102 (52): 10650-10657.

[46] Yeung, K. L., Maira, A. J., Stolz, J., Hung, E., Ho, N. K.-C., Wei, A. C., Soria, J., Chao, K.-J., Yue, P. L. (2002). Ensemble Effects in Nanostructured TiO_2 Used in the Gas-Phase Photooxidation of Trichloroethylene. *J. Phys. Chem. B,* 106 (18): 4608-4616.

[47] Zhang, H., Chen, B., Banfield, J. F., Waychunas, G. A. (2008). Atomic Structure of Nanometer-Sized Amorphous TiO_2. *Phys. Rev. B: Condens. Matter Mater. Phys.,* 78 (21): 214106/1-214106/12.

[48] Bartholomew, C. H., Farrauto, R. J. (2003). *Fundamentals of Industrial Catalytic Processes*. John Wiley & Sons: p 700 pp.

[49] Peng, J., Wang, S. (2007). Performance and Characterization of Supported Metal Catalysts for Complete Oxidation of Formaldehyde at Low Temperatures. *Appl. Catal., B,* 73 (3-4): 282-291.

[50] Kimura, K., Einaga, H., Teraoka, Y. (2010). Catalytic Properties of Platinum Supported on Titanium Dioxide by Liquid-Phase Adsorption of Colloidal Nanoparticles. *Catal. Lett.,* 139 (1-2): 72-76.

[51] Iida, H., Yonezawa, K., Kosaka, M., Igarashi, A. (2009). Low-Temperature Water Gas Shift Reaction Over Pt-Re/TiO_2 Catalysts Prepared by a Sub-Critical Drying Method. *Catal. Commun.,* 10 (5): 627-630.

[52] Li, Z., Meng, M., You, R., Ding, T., Li, Z. (2012). Superior Performance of Mesoporous TiO_2-Al_2O_3 Supported NSR Catalysts with the Support Synthesized Using Nonionic and Cationic Surfactants as Co-Templates. *Catal. Lett.,* 142 (9): 1067-1074.

[53] Karatzas, X., Jansson, K., Gonzalez, A., Dawody, J., Pettersson, L. J. (2011). Autothermal Reforming of Low-Sulfur Diesel Over Bimetallic RhPt Supported on Al_2O_3, CeO_2-ZrO_2, SiO_2 and TiO_2. *Appl. Catal., B,* 106 (3-4): 476-487